Digest Journal of Nanomaterials and Biostructures Vol. 14, No. 1, January - March 2019, p. 109 - 117

# EFFECT OF SURFACTANTS ON MORPHOLOGY AND PHOTOLUMINESCENCE PROPERTIES OF $SrMoO_4:Dy^{3+}$ PHOSPHORS

L. ZHANG[a,b,*], G. ZHENG[b], Z. DAI[b], H. LI[a], Z. YU[a]

[a]*Department of Chemical and Material Engineering, Hefei University, Hefei 230601, China*

[b]*Anhui Key Laboratory of Information Materials and Devices, School of Physics and Materials Science,Anhui University, Hefei 230039, China*

Using sodium citrate ($Na_3Cit$) and polyethylene glycol (PEG4000) as surfactants, $SrMoO_4:0.01Dy^{3+}$ phosphors were prepared by hydrothermal method. The structure, morphology and luminescent properties are investigated by X-ray diffraction (XRD), scanning electron microscope (SEM), and fluorescence spectrometer. Our results suggest that these surfactants do not change the crystal structure of $SrMoO_4$ phosphors. However, the morphologies of $SrMoO_4$ phosphors are greatly influenced with the introduction of these surfactants.With $Na_3Cit$ or PEG addition, the flake-like morphology of $SrMoO_4:0.01Dy^{3+}$ is changed into the spindle- and flower-like one. The most intense emission is observed to be located around 576nm due to $^4F_{9/2}\rightarrow{}^6H_{13/2}$ transition of $Dy^{3+}$. The emission intensity is quenched for $Na_3Cit$-added sample. For PEG-added samples, with increasing amounts of PEG, the emission intensity is firstly enhanced and then lowered. The maximum emission intensity is achieved when the molar ratio of PEG to Sr is 0.5:1.

(Received September 19, 2018; Accepted February 14, 2019)

*Keywords*: Molybdates, Surfactants, Morphology, Luminescence

## 1. Introduction

Metal molybdates is one important family of inorganic material with great potential applications in various fields, including phosphors, optical fibers, scintillators, magnets and catalysts [1,2].In these molybdates, $SrMoO_4$ (SMO) especially attracted enormous attention, since SMO exhibits excellent luminescence properties within the blue and green spectral regions. And then SMO has great potential utilities in self-activated luminescent material and devices [3]. In particular, with the doping different rare-earth ions, the luminescence properties of these molybdates are changed correspondingly. In previous reports, it is found that those molybdates samples with $Eu^{3+}$, $Sm^{3+}$, $Tb^{3+}$, and $Dy^{3+}$ ions dopants have broad and intense absorption bands [4-8]. Therefore, the rare-earth element doping is generally used to tune the luminescent properties of the SMO system.

* Corresponding author: 522671714@qq.com

As for the synthesis of SMO nanostructures, up to now, different preparation methods are adopted to obtain SMO samples. These methods include the co-precipitation reaction [9], the microwave radiation [10], the electrochemical process [11], the hydrothermal method [12].Then various micro/nanostructural $SrMoO_4$, such as nanowire, flower-like mesocrystal, ellipsoidal rods, peanuts, dumbbells, peaches, rice-like nanostructures have been successfully synthesized via these different methods and techniques [13-18]. In these preparation methods, since surfactants have electrostatic repulsion and steric hindrance, the surface tension of the solution can be reduced correspondingly. The growth of grain will be hindered and the formation of aggregats can also be prevented. As a result, the morphology and optical properties of phosphors would be effected. Using different surfactants, some phosphors with different morphologies were obtained by hydrothermal process [19,20]. Xu et al also reported that the surfactants play a key role in controlling of the sample morphology [21]. In addition, it is observed that the surfactants can be used as the template to control the surface morphology of phosphors and enhance the luminescent efficiency [22].

It is well known that it is very important to probe the possible quantitative relation between the surfactants molar ratio and the luminescent performance, and the effect of different surfactants molar ratio on the luminescent properties. Therefore, using $Na_3Cit$ and PEG4000 as surfactants, $SrMoO_4$:0.01$Dy^{3+}$ phosphors are prepared by hydrothermal method in the current work. The effect of surfactants on the morphology and the luminescent properties of the samples are also systematically probed. Our results clearly suggest that $Na_3Cit$ and PEG are both favorable for the formation of spindle-like structure. The possible formation mechanism is also put forward on the basis of experimental results. As for the luminescent performance, it is observed that the emission intensity is lowered with a certain amount of $Na_3Cit$ addition. More interestingly, for these samples with PEG addition, the emission intensity is firstly increased and then decreased with increasing PEG amount. When the molar ratio of PEG to Sr is 0.5:1, one maximum emission intensity is achieved.

## 2. Experimental

$SrMoO_4$:0.01$Dy^{3+}$ phosphors were synthesized using hydrothermal method. The following raw materials $Sr(NO_3)_2$(≧99%), $Na_2MoO_4{\cdot}2H_2O$, $Dy(NO_3)_3{\cdot}6H_2O$, $Na_3Cit$, NaOH, Polyethylene glycol(PEG4000) and de-ionized water were used in our synthesis process. At first, stoichiometric amounts of $Sr(NO_3)_2$, $Na_2MoO_4{\cdot}2H_2O$ and $Dy(NO_3)_3{\cdot}6H_2O$ were dissolved in the deionized water to form aqueous solutions of the individual raw materials, respectively. The $Sr(NO_3)_2$ and $Dy(NO_3)_3$ solutions were dropped to the aqueous $Na_2MoO_4$ solution slowly under stirring. Then NaOH solution was added dropwise to adjust the pH of the resultant mixed solution to 6. Finally, the mixture was placed in a 50ml capacity, Teflon-lined stainless-steel autoclave and heated at 100℃ for 6h. After the autoclave was cooled to room temperature naturally, the products were separated by centrifugation, washed with ethanol and deionized water several times, and dried at 80℃to obtain powders. The as-prepared product was denoted as sample **S1**. Based on the obtained sample S1, an amount of $Na_3Cit$ ($Na_3Cit$/Sr=3:1) was added. The obtained sample was labeled as S2. Similar to S2, **S3-S7** were prepared with different molar ratios of PEG:Sr addition in sample S1. The PEG was added to the mixed solution under stirring for 60min at 40°C. All these obtained

samples under different experimental conditions are summarized in Table 1.

*Table 1. Various surfactant and the corresponding obtained samples.*

| Sample | S1 | S2 | S3 | S4 | S5 | S6 | S7 |
|---|---|---|---|---|---|---|---|
| $Na_3Cit$:Sr(mol) | -- | 3:1 | -- | -- | -- | -- | -- |
| PEG:Sr(mol) | -- | -- | 0.5:1 | 1:1 | 2.5:1 | 3:1 | 4:1 |

The crystal structure of the products was characterized by X-ray diffraction using an X-ray diffractometer (XRD dx-2000 SSC) with Cu Kα radiation (λ=1.5406Å) over a scanning range of 10-80º with a step of 0.02º. Scanning electron microscopy (SEM, S-4800, Hitachi) was also used to observe the morphology and the microstructure. The excitation and the emission spectra were measured on a fluorescence spectrophotometer (F-4500, Hitachi). All these measurements were carried out at room temperature.

## 3. Results and discussion

### 3.1. Structures

In Fig. 1, the XRD patterns for S1 and S2 (a) and S1-S7 (b) samples are presented. It is observed that all these XRD patterns can be well indexed as the pure scheelite tetragonal structure ($I4_1/a$ space group). These results are in good agreement with the values of the standard card (JCPDS 08-0482). Therefore, the introduction of surfactants does not change the host crystal-structure of $SrMoO_4$:0.01$Dy^{3+}$ phosphors.

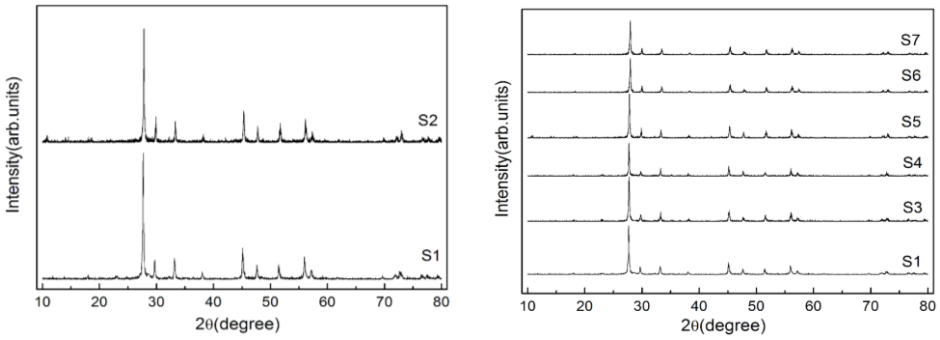


*Fig. 1. (a) XRD patterns of S1 (without-$Na_3Cit$) and S2 (with-$Na_3Cit$) samples (b) XRD patterns of S1 (without-PEG) and S3-S7 (with-PEG) samples.*

The average crystallite sizes of all samples were calculated using Debye-Scherrer equation, $D=0.9\lambda/(\beta\cos\theta)$. In this formula, $D$ denotes the average crystallite size, and $\lambda$(=1.5406Å) is the wavelength of incident X-ray. $\beta$ is the corrected full width at half-maximum (FWHM), and $\theta$ is the diffraction angle for the (h k l) plane. For S1-S7 samples, the calculated crystallite sizes are 50.17, 48.31, 50.27, 63.48, 73.59, 59.79, and 35.65nm, respectively. Based on the calculated crystallite

sizes, it is clearly found that, via $Na_3Cit$ addition, the crystallite size of the sample may become small. However, with the addition of PEG addition, the $SrMoO_4$:$Dy^{3+}$ crystalline size firstly increases from 50.17 to 73.59nm. Then, the crystalline size decreases from 73.59 to 35.65nm with increasing PEG addition further. Therefore, the variation of the crystallite size with the PEG addition is not continuous and monotonous.

### 3.2. Morphologies

Fig. 2 (a) and (b) present the morphologies of **S1** and **S2** samples. For the samples without $Na_3Cit$ addition,as shown in Fig. 2(a), some nanosheets are observed to overlap each other irregularly. With an amount of $Na_3Cit$ being added into the precipitator, the morphologies begin to change gradually. The as-obtained samples are in the form of spindles. Obviously, the $Na_3Cit$ addition plays an important role in the morphology formation. The $Cit^{3-}$ is one strong chelating agent with three carboxylate groups for $Sr^{2+}$ ions, and form $Sr^{2+}$-$Cit^{3-}$ complexes. The chelating of the $Sr^{2+}$-$Cit^{3-}$ complex is attacked by $MoO_4^{2-}$ and anion-exchange reaction between $MoO_4^{2-}$ and $Cit^{3-}$ would take place, and then $Sr^{2+}$ is released. With the two microemulsions being mixed together, the reaction between the $Sr^{2+}$ and $MoO_4^{2-}$ begins. As the consequence of homogenous nucleation in the system, it directly results in the small $SrMoO_4$ nanoparticles.Then, these single $SrMoO_4$ nanoparticles grow into ultrathin and irregular nanoflakes in the solution through oriented attachment. Finally, in order to further decrease the overall energy, the ultrathin nanoflakes start to self-assemble to the spindles by layer-by-layer attachment. The spindle-like morphology can be observed by further growth as shown in Fig. 2(b).

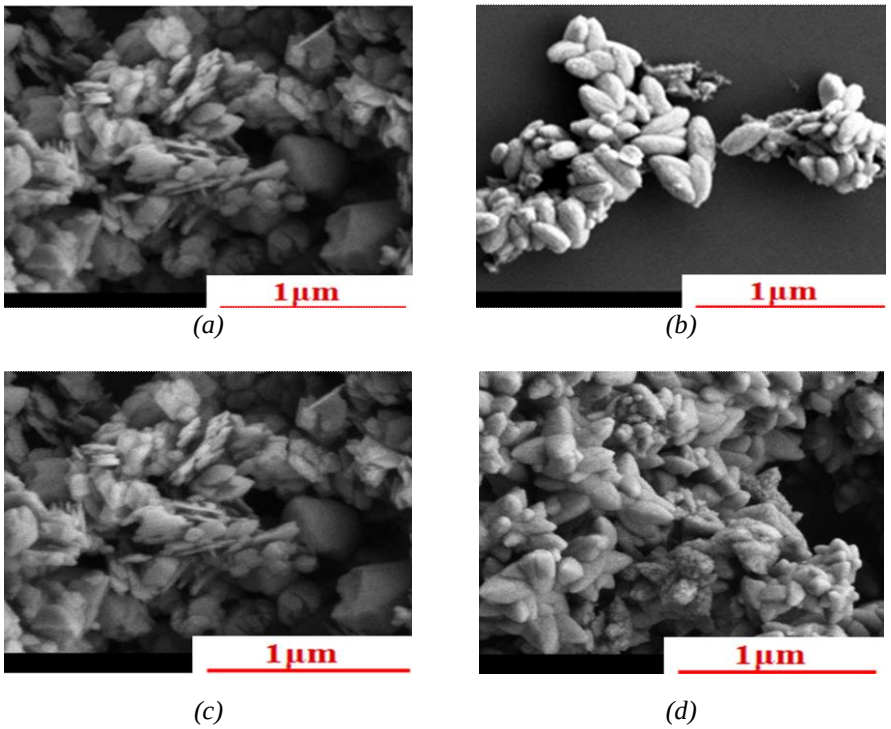


*(a)* *(b)*

*(c)* *(d)*

*Fig. 2. (a) (b)SEM images of S1 (without-$Na_3Cit$) and S2 (with-$Na_3Cit$) samples; (c) (d)SEM images of S1 (without-PEG) and **S3** (with-PEG) samples.*

As we know, the morphology and the growth kinetics of the phosphor particles are influenced by the PEG addition. In the case of ZnO nanostructure, PEG controls the growth rates of the colloids in a certain direction, assisting the formation of unidirectional nanowires and nanorods [23]. The effect of surface modification by PEG was interpreted as local structural rearrangement of activator centers at YAG nanocrystals [24]. These results indicate that the polymer-assisted synthesis yields modified surface conditions. Fig. 2 (c) and (d) present the morphology of **S1** and **S3** samples. With an amount of PEG being added in the solution, the sheet-like structures disappear, but the spindle structures appear. Then, these spindles begin to aggregate and the flower-like structures are formed. Moreover, it is observed that these as-prepared particles show uniform distribution and that the sizes of these particle range from 100 to 500nm.The particles of phosphors seem to be second aggregation of the crystalline, thus the particle sizes obtained by SEM images are bigger than the calculated crystallite sizes. When PEG is added into the solution, PEG with the long-chain stretche in the solution is absorbed on the $SrMoO_4$:0.01$Dy^{3+}$ particle surface. And it controls the degree of the surface reactivity, which finally modifies the growth kinetics and/or leads to the anisotropicly shaped nanostructure[23].To be more specific, via the PEG chains those the primary $SrMoO_4$:0.01$Dy^{3+}$ particles, which are scattered in a certain scope, will move close,link together, and assemble into flower-like structures. These flower-like structures are presented in Figure 2(d). In addition, it is worth pointing out that the morphologies of **S4**-**S7** samples can't be detected well, which may be ascribed to the encapsulation PEG layer on the samples surface. Based on the above discussions, our results clearly reveal that the $Na_3Cit$ and the PEG additions are both beneficial to the formation of the spindle-like and the flower-like structures.

### 3.3. Luminescent properties

Fig. 3 (a) and (b) show the excitation spectra of $SrMoO_4$:0.01Dy phosphor (**S1** and **S2** samples). These spectra were recorded in the range of 340~500nm by monitoring the emission at 576nm corresponding to the $^4F_{9/2}\rightarrow{}^6H_{13/2}$ transition. It is clearly observed that the excitation profiles do not change with the addition of $Na_3Cit$. The excitation spectra exhibits six bands, which are centered at 356, 368, 393, 432, 456, and 480nm. These bands are due to the transitions from $^6H_{15/2}$ ground state to $^6P_{7/2}$, $^6P_{5/2}$, $^4F_{7/2}$, $^4G_{11/2}$, $^4I_{15/2}$, and $^4F_{9/2}$ excited states, respectively. The corresponding emission spectra of $SrMoO_4$:0.01$Dy^{3+}$ phosphors, which are recorded by exciting at 368nm, are shown in Figure 3(b). The intense emission bands at 486nm and 576nm are assigned to $^4F_{9/2}\rightarrow{}^6H_{15/2}$ and $^4F_{9/2}\rightarrow{}^6H_{13/2}$ transitions, respectively. It is also observed that, both excitation and emission intensity of $Dy^{3+}$ are decreased with addition of $Na_3Cit$.

Fig. 3(c) and (d) present the excitation and emission spectra of $SrMoO_4$:0.01Dy phosphor (S1, S3-S7 samples). Irrespective of the addition of PEG, it is found that there is no significant difference in the shape or the band position of the PL spectra, However, as for the S3 sample, it is observed that the emission intensity is enhanced with the addition of PEG. This is due to local structural rearrangement of activator centers at phosphors, induced by PEG [24]. Zhou et al also reported that a certain amount of PEG is necessary to obtain optimum emission intensity [25]. When the ratio of PEG to Sr is 0.05:1, based on the XRD and SEM results, it is observed that there exist appreciable changes in the average particle size and the morphology of the samples. Therefore, it may be deduced that the enhancement of emission intensity is due to the crystallites and the morphology change. When PEG is added into the solution, one hand of PEG long-chain

stretches adequately, and the other hand absorbs on the $SrMoO_4:Dy^{3+}$ particle surface. Thus, the PEG-assisted hydrothermal process yields the surface stabilized particles by the formation of PEG-OH bonds. As a result, the emission intensity is enhanced with certain amount PEG addition. However, the emission intensity is decreased with increasing PEG addition further. This can be understood in terms of the modified surface properties in conjunction with the induced encapsulation layer, as discussed in the SEM part. In our preparation process, a certain amount of $OH^-$ are coordinated to $Dy^{3+}$ particles on the surface and these hydroxyl groups act as the multiphonon relaxation centers. The poor luminescence efficiency may arise from various pathways of non-radiative relaxation for nanomaterials [26, 27]. In addition, with more PEG is added into the solution, these PEG4000 long chains intertwine each other, making these $SrMoO_4:0.01Dy^{3+}$ particles aggregate heavily. As a result, the emission intensity is lowered.

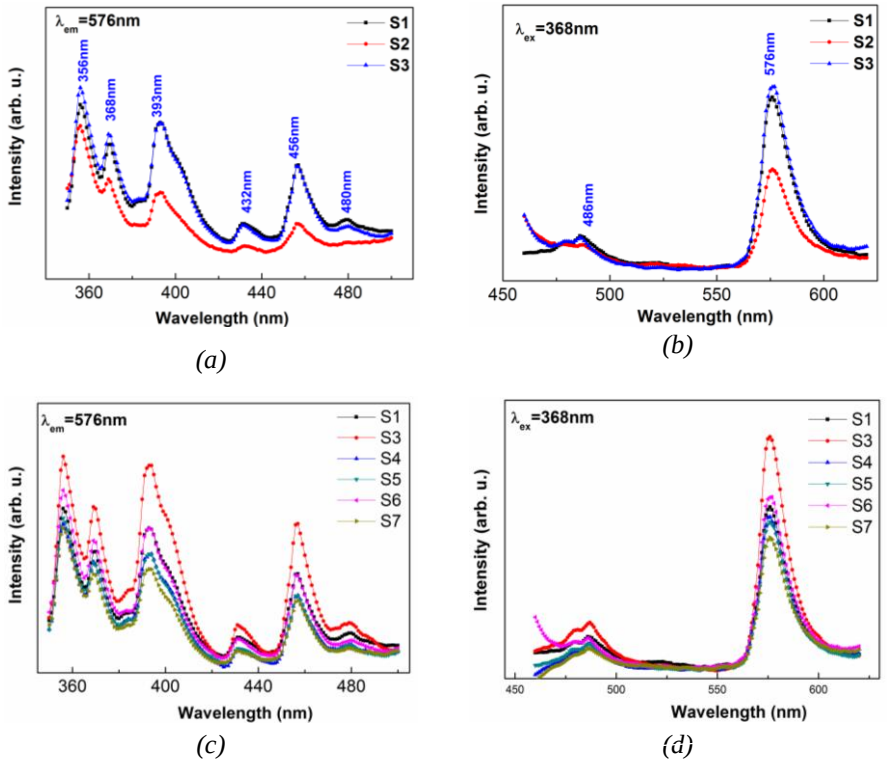


*Fig. 3. (a) Excitation spectra (S1, S2 and S3 samples) for monitoring with $\lambda_{em}$=576nm of $SrMoO_4$:0.01Dy sample; (b) Emission spectrum (S1, S2 and S3 samples) of $SrMoO_4$:0.01Dy samples under 368nm excitation; (c) Excitation spectra (S1, S3-S7 samples) for monitoring with $\lambda_{em}$=576nm of $SrMoO_4$:0.01Dy sample;(d) Emission spectrum (S1, S3-S7 samples) of $SrMoO_4$:0.01Dy samples under 368nm excitation.*

Generally, the intensity ratio of electric dipole (ED) and magnetic dipole (MD) transitions ($I_{ED}/I_{MD}$) can be used to understand the symmetry of local environment of the trivalent 4f ions in the host matrix. When the ratio is higher, the site symmetry is lower. As for our samples, the intensity ratio of luminescence *I* ($I=I_{(4F9/2\rightarrow6H13/2)}/I_{(4F9/2\rightarrow6H15/2)}$ for $Dy^{3+}$) was calculated from the emission spectrum. For these samples, the ED transition $^4F_{9/2}\rightarrow{}^6H_{13/2}$ is only allowed electric dipole transition when $Dy^{3+}$ located at a site of non-inversion symmetry, while $^4F_{9/2}\rightarrow{}^6H_{15/2}$

magnetic dipole transitions is at a site of inversion symmetry. The fact that yellow emission at 576nm ($^4F_{9/2}\rightarrow{}^6H_{13/2}$) is predominant which suggests that the local environment around dysprosium lacks inversion symmetry in all samples. The ratio of $^4F_{9/2}\rightarrow{}^6H_{13/2}$ to $^4F_{9/2}\rightarrow{}^6H_{15/2}$ for **S1**-**S7** samples is calculated to be 2.7851, 2.0993, 3.1401, 2.9189, 2.8835, 2.9753, and 2.8336, respectively (Table 2). Comparing **S1** with **S2**, the result indicates that the symmetry around $Dy^{3+}$ increases with $Na_3Cit$ addition. The intensity of the ED transition and the MD transition ($I_{ED}/I_{MD}$) firstly increases, then it decreases with increasing PEG.

*Table 2. R/O ratios and CIE coordinates for all samples.*

| Sample | | S1 | S2 | S3 | S4 | S5 | S6 | S7 |
|---|---|---|---|---|---|---|---|---|
| R/O | | 2.7851 | 2.0993 | 3.1401 | 2.9189 | 2.8835 | 2.9753 | 2.8336 |
| CIE | x | 0.3924 | 0.3667 | 0.4015 | 0.4048 | 0.3986 | 0.3938 | 0.4048 |
| | y | 0.4516 | 0.4338 | 0.4478 | 0.4597 | 0.4566 | 0.4396 | 0.4637 |

Chromaticity coordinates is one of the important factor in evaluating the performance of the prepared phosphors. So the chromaticity coordinates of our samples have been calculated. Our calculations are based on the corresponding emission spectrum from Fig. 3, using the CIE 1931 color matching functions. The chromaticity coordinates are presented in Fig. 4. It can be clearly seen that most chromaticity coordinates are located in the white-light region. With $Na_3Cit$ and PEG addition, the color changes gradually.

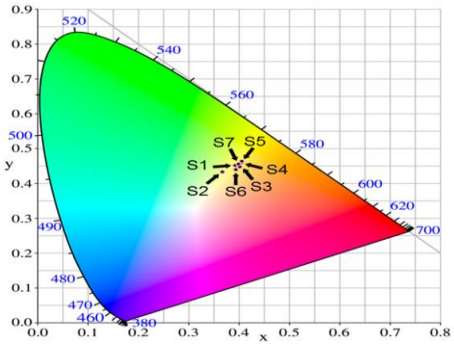


*Fig. 4. CIE images for S1-S7 samples.*

## 4. Conclusions

Via hydrothermal method, $SrMoO_4$:0.01$Dy^{3+}$ phosphors were synthesized using sodium citrate ($Na_3Cit$) and polyethylene glycol (PEG4000) as surfactants. The morphology, the structure, and the luminescent properties are systematically investigated by XRD,SEM, and fluorescence spectrometer. The results suggest that the surfactants play an important role in controlling the morphology and luminescent properties of $SrMoO_4$:0.01$Dy^{3+}$ phosphors. With $Na_3Cit$ or PEG addition, the flake-like morphology of $SrMoO_4$:0.01$Dy^{3+}$ is changed into the spindle- and flower-like one. The most intense emission is observed to be located around 576nm due to $^4F_{9/2}\rightarrow{}^6H_{13/2}$ transition of $Dy^{3+}$. The emission intensity is quenched for $Na_3Cit$-added sample.

However, for PEG-added samples, the emission intensity is enhanced firstly and then lowered with increasing PEG amount. The maximum emission intensity is achieved when the ratio of PEG to Sr is 0.05:1.

## Acknowledgments

This work was financially supported by the National Natural Science Foundation of China under Grant no.11204001, Natural Science Foundation of Anhui Province (1308085MA04), Key Research and Development Projects of Anhui Province(1804A09020096), and the Higher Educational Natural Science Foundation of Anhui Province (KJ2017A534).

## References

[1] M. V. Raskina, V. A. Morozov, A. V. Pavlenko, I. G. Samatov, I. V. Arkhangelskii, S. Y. Stefanovich, B. I. Lazoryak, Russ. J. Inorg. Chem. **60**, 84 (2015).
[2] Y. L. Yang, X. M. Li, W. L. Feng, W. J. Yang, W. L. Li, C. Y. Tao, J. Alloys. Compds. **509**, 845 (2011).
[3] M. Niklm, P. Bohacek, E. Mihokova, M. Kobayashi, J. Lumin. **87**, 1136 (2000).
[4] S. L. Wei, L. X.Yu, F. H. Li, J. J. Sun, S. C. Li, Ceram. Int. **41**, 1093 (2015).
[5] L. L. Li, Z. H. Leng, W. W. Zi, S. C. Gan, J. Electron. Mater. **43**, 2588 (2014).
[6] S. K. Gupta, M. Sahu, P. S. Ghosh, D. Tyaqi, M. K. Saxena, R. M. Kadam, Dalton Trans. **44**,18957 (2015).
[7] Z. W. Zhang, X. H. Shen, Y. J. Ren, W. L. Hou, W. G. Zhang, D. J. Wang, Opt. & Laser Tech. **56**, 348 (2014).
[8] M. Ghaed-Amini, M. Bazarganipour, M. Salavati-Niasari, J. Mater. Sci.:Mater. Electron. **26**, 7452 (2015).
[9] L. Y. Zhang, W. W. Fu, G. H. Zheng, Z. X. Dai, Y. N. Zhu, J. J. Mu, J. Mater. Sci.: Mater. Electron. **27**, 5164 (2016).
[10] T. Thongtem, A. Phuruangrat, S. Thongtem, Mater. Lett. **62**, 454 (2008).
[11] Y. Sun, J. F. Ma, J. R. Fang, C. Gao, Z. S. Liu, Inorg. Chem. Commun. **14**, 1221 (2011).
[12] L. L. Lin, R. Q. Li, W. W. Zi, S. C. Gan, Phys. B: Conds. Mater. **458**, 8 (2015).
[13] F. Achour, S. Corbel, L. Balan, K. Mozet, E. Girot, G. Medjahdi, M. Ben-Said, A. Ghrabi, Mater. & Design **101**, 309 (2016).
[14] R. C. Monreal, T. J. Antosiewicz, S. P. Apell, J. Phys. Chem. C **120**, 5074 (2016).
[15] H. L. Guo, Q. Zhu, X. L.Wu, Y. F. Jiang, X. Xie, and A. W. Xu, Nanoscale **7**, 7216 (2015).
[16] Z. W. Zhang, X. H. Shen, Y. J. Ren, W. L. Hou, W. G. Zhang, D. J. Wang, Opt. Laser Tech. **56**, 348 (2014).
[17] G. J. Xing, Y. M. Li, Y. L. Li, Z. L. Wu, P. Sun, Y. Wang, C. Zhao, G. M. Wu, Mater. Chem. Phys. **127**, 465 (2011).
[18] T. Thongtem, A. Phuruangrat, S. Thongtem, Mater. Sci. **27**, 43 (2009).
[19] B. Yan, J. F. Gu, J. Alloys. Compd. **479**, 536 (2009).
[20] Y. N. Zhu, W. W. Fu, P. F. Zhang, G. H. Zheng, J. J. Mu, L. Y. Zhang, J. Mater. Sci.: Mater.

Electron. **27**, 12772 (2016).
[21] Z. H. Xu, X. J. Kang, C. X. Li, Z. Y. Hou, C. M. Zhang, D. M. Yang, G. G. Li, J. Lin, Inorg. Chem. **49**, 6706 (2010).
[22] X. Y. Chang, C. Ma, Opt. Mater. **32**, 415 (2010).
[23] Z. Q. Li, Y. Z. Xiong, Y. Xie, Inorg. Chem. **42**, 8105 (2003).
[24] T. Isobe, Phys. Status Solidi A **203**, 2686 (2006).
[25] Y.H. Zhou, J. Lin, Opt. Mater. **27**, 426 (2005).
[26] S. H. Choi, Y. M. Moon, H. K. Jung, J. Lumins. **130**, 549 (2010).
[27] S. Cao, Y. Q. Ma, C. M. Quan, W. L. Zhu, W.J. Yin, K. Yang, G. H. Zheng, M. Z. Wu, Z. Q. Sun, J. Alloys. Compd. **487**, 346 (2009).